Proceedings of the ASME 2020 International Design Engineering Technical Conferences & Computers and Information in Engineering Conference
IDETC/CIE 2020
August 16-19, 2020, St. Louis, MO, USA

DETC2020-22321

DESIGN AND DEVELOPMENT OF HARDWARE TO ANALYZE AND CATEGORIZE THE CONDITION OF BATTERIES WITH THE AIM OF ENABLING THEIR RE-USE

Andrew Wilson
Department of Engineering
Durham University
Durham, United Kingdom

Qing Wang
Department of Engineering
Durham University
Durham, United Kingdom

ABSTRACT

This paper covers the design and implementation of an accurate, yet flexible test system for Lithium-Ion batteries. The system makes use of linear charge and discharge circuitry to ensure a low noise control, and can support the simultaneous and independent testing of six cells. The system is controlled and data collected by specialist MatLab© software with a user-friendly GUI. Experimental data is processed within the same environment to obtain the desired information. The system makes use of Full Cycle Coulomb Counting and Pulsed DC Load Analysis to obtain estimates for the State of Health (SoH) and State of Charge (SoC) of various cells, and to examine the effect of different use cases on cell performance through repeated testing.

1. INTRODUCTION

Batteries it can be said make the world go round, relied upon every day to power a multitude of devices, from cars to cellphones. Although non-rechargeable chemistries continue to offer superior capacities, the market share of rechargeable batteries in particular continues to grow as the use and power demands of portable devices increases. This has led the cost equation to significantly favor rechargeable over non-rechargeable batteries [1].

Over the years many different rechargeable chemistries have been developed, the three most common in use today being: Lead-Acid, Nickel Metal Hydride (NiMH) and Lithium-Ion (Li-Ion) based chemistries.

Devices where portability is a priority, necessitate batteries of small size and light weight. It is in this category that Li-Ion batteries (LIBs) reign supreme, with significantly better performance than both NiMH and Lead-Acid in nearly every category (except price), as shown in Table 1 below.

Table 1: Comparison of Li-ion, NiMH, and Lead-Acid cells [2]

Property	Li-Ion	NiMH	Lead-Acid
Gravimetric Energy Density (Wh/kg)	100 - 250	60 - 120	30 - 50
Gravimetric Power Density (W/kg)	250 - 800	250-500	150-200
Volumetric Energy Density (Wh/L)	250 - 700	140 - 300	80 - 90
Ideal Charge Rate	0.5C	0.2C	0.05C
Peak Discharge Rate	2 - 30C	~5C	~5C
Ideal Discharge Rate	1 - 10C	~0.5C	~0.2C
Cycle Efficiency	~97%	~80%	~90%
Cycle Life	500-2000	300 - 500	200 - 300

This monopoly is only set to endure with the price of LIBs continuing to reduce at an accelerated rate, spurred on by new markets and economy of scale [2,3]. The effect of ever greater LIB production, however, is naturally ever greater waste. As the capacity of LIBs fades gradually with use (discussed in Section 2.3) there comes a point where the runtime that they are able to provide becomes too short to facilitate their continued use. The point at which this occurs naturally depends on user tolerance and the application, however for the purpose of warranty administration and industry testing it is commonly set at 80% of the nominal capacity [3].

It is important to note that although the capacity of LIBs will fade over time, the cycle efficiency (energy out compared to energy in) does not suffer to any great degree [2]. As such it naturally follows that in some applications this may result

in a significant loss in function, whereas for others the change may not be a significant problem. It is worth noting that a LIB with only 80% of its nominal capacity will still have upwards of twice the performance of a Lead-Acid of comparable size.

Since LIBs are resource intensive to manufacture, both in terms of raw materials and energy, methods that increase their life cycle efficiency by repurposing old batteries (with remaining useful life) to other applications have great potential [4], for example, in mains power grid demand levelling, where energy density is not generally of chief concern [5].

Research has shown that end users tend to expect more from batteries than they can reasonably provide [2]. In some applications (notably those where devices are subject to a full discharge, i.e. cellphones) even a small drop in capacity can create significant problems for the user. This can result in the assumption that capacity has dropped to a greater degree than reality [2]. Additionally, a lack of understanding about now a device uses power may lead to lower runtimes than expected (e.g. the effects of software updates, or background tasks). This contributes to the early retirement of otherwise perfectly healthy batteries, with one study finding as many as 90% of returned cellphone batteries had no ascertainable issues [2].

As is explored further in Sections 2.1 and 2.3, some of the qualities that make LIBs so well suited for portable applications together with the form of usage itself, can cause problems when it comes to accurately measuring the capacity of, and charge remaining in, a cell. Commentators generally agree that consistently accurate and dependable battery monitoring is still far from reality [6]. This leads to another important factor affecting waste, that being the effect of user uncertainty.

In some applications (notably those involving mission critical yet irregular use, e.g. emergency medical devices or uninterruptable power supplies) uncertainty over the capacity of cells can also lead to their early retirement for fear that performance might not be up to standard [2].

Uncertainty about the level of charge can have more substantial consequences, for example, it may result in a device cutting out unexpectedly at an important moment, or requiring the user to shutdown devices early (and perhaps unnecessarily) for fear of unexpected sudden power depletion. In fact, evidence indicates that user uncertainty over charge remaining, aside from causing user confusion and frustration, can actually lead users to subject batteries to more abuse than necessary i.e. charging a battery repeatedly or for too long when not required [7]. Accurate testing methods are therefore essential to reducing needless battery waste, and enabling the possible reuse of cells in other areas (e.g. grid levelling), before recycling. Research into battery monitoring is split into several different areas with effort being made to reduce the trade-offs between complexity, speed, and accuracy present in each. Research on several notable approaches, their methodology, complexity and accuracy are outlined in detail in Section 2.5.

The aim of this research was to design an accurate and flexible battery test platform that could be used to gather more extensive experimental data, and permit a wider selection of test formats, before using this to analyze and verify various test formats (including constant and pulsed DC loading). This would benefit research into the development of an effective testing and classification procedure, taking into account possible trade off in the accuracy versus speed of tests, and process efficiency.

An overview of battery theory including electrical models of behavior, together with characteristics, modes of failure and testing, is given in Section 2. A detailed explanation of the test system design and operation methodology follows in Section 3. Section 4 covers the verification of system function and analysis of experimental data collected, leading to an examination of effectiveness of different test methods.

2. BATTERY TESTING THEORY

Batteries are complex electro-chemical devices, the study of which has evolved and advanced over decades. A cell's response is a combination of various chemical, physical and electrical processes, which evolve and change with time and use, a factor that frustrates research [8].

2.1 Battery Terminology

Common battery terminology is a complicated and imprecise business, based to a large degree on historic use cases and priorities. Many values are interdependent, varying according to not only the specific cell chemistry and structure, but also the way a cell is used.

Nominal voltage is given by the manufacturer and is based on the average voltage maintained by a battery during a discharge, normally at modest current. LIBs are notable for their extremely flat voltage curves (see Figure 10) compared to other chemistries [3]. A quality that brings both advantages and disadvantages (discussed in Section 2.5). The larger the load, the faster the voltage drops and the lower the average voltage is across the discharge curve (explained further in Section 2.4).

Maximum Instantaneous Power (MIP) is the maximum power that a cell can provide at any moment, generally measured from a rested state. It is related to the more traditionally quoted Cold Cranking Amp (CCA), a term derived from the automotive industry describing the maximum current that a rested cell can provide. The MIP is dependent fundamentally on a cell's chemistry and structure, along with its SoC and, to a lesser degree, SoH.

Since modern electronics generally make use of efficient switch-mode power supplies over the older linear regulators, for a fixed load, power flow becomes the constant quality, as current drawn from the cell is increased during discharge to compensate for the dropping voltage. MIP may be more helpful in modern applications than CCA.

Discharge Cut-off Voltage (DCV) is the loaded cell voltage that when reached is considered to indicate when a cell is fully discharged. The level of cut-off is normally determined by the size of load together with concern for longevity (discussed further in Section 2.3).

Charge Cut-off Voltage (CCV) is the voltage to which a cell is charged and is set primarily dependent upon a cell's chemistry, and as discussed further in Section 2.3 represents a compromise between capacity and longevity.

C-Rate is a measure of rate of charge or discharge of a battery as a product of its nominal capacity. It can be translated to current by Equation 1 below:

$$Current\ (A) = Nominal\ Capacity\ (A\square) \times C\text{-}Rate. \quad (1)$$

Capacity is a measure of the amount of energy stored by a battery. It is traditionally given in terms of AmpHours (Ah). This can, however, be somewhat misleading, as the actual energy outputted by the cell is dependent on its voltage over discharge (a quality not fixed, as already discussed). The greater the current the cell must provide, the greater the voltage drop, and the less total energy can be extracted as result. Therefore, WattHours (Wh) is often a more informative if similarly imprecise term, particularly when considering modern electronics, if more technically involved.

Nominal capacity is the capacity quoted by the manufacturer and is based on the energy extracted during a discharge at modest current (generally 0.2C [2]).

State of Charge (SoC) is a measure generally quoted in terms of a percentage of the amount of energy that is stored within a cell relative to its actual capacity (the energy stored within it when fully charged).

State of Health (SoH) is a measure of the degree of capacity fade experienced by a cell (discussed in Section 2.3). It is commonly quoted as the percentage of nominal capacity that remains (at a given discharge rate) given by Equation 2 below.

$$SOH = \frac{Actual\ Capacity}{Nominal\ Capacity} \quad (2)$$

SoH can also be considered in terms of the amount of instantaneous current or power that it can provide compared to nominal. However, gradual fade in these terms is generally much less dramatic, especially in LIBs.

2.2 Li-Ion Electrochemical Cells

Li-Ion cells rely on the principle of the transfer of positive lithium ions (Li_+) through an electrolyte from one electrode to another. The anode (generally graphite) acts like a sponge, and in a charged state holds the lithium atoms within its structure [3]. When a cell is discharged, the lithium in the anode gives up an electron, creating an electric current. The Li_+ defuse into the electrolyte and over to the cathode (a metal oxide), where it regains an electron and is held within its structure. The chemical gradient between the anode and the cathode determines the potential difference [3].

A battery's performance is the product of both the chemical structure (in terms of the mix of metal oxides and electrolyte) and physical structure (spacing between electrodes, and atomic structure of the electrodes themselves). The mix of oxides and their structure controls the rate and degree of acceptance of the Li_+, whereas the electrolyte and spacing determines the ease of ion flow. Both have a strong impact on a cell's capacity and MIP.

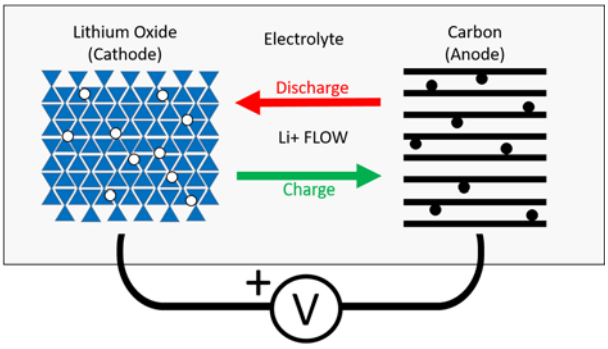

Fig.1: Ion flow within a Li-ion cell [2]

As previously mentioned, Li-Ion comprises a broad family of different but related chemistries including: Lithium Cobalt Oxide (LCO), Lithium Iron Phosphate (LIP), Lithium Manganese Oxide (LMO), and Lithium Nickel Manganese Cobalt Oxide (NMC). Each chemistry has its own strengths and weaknesses, however NMC cells (developed later around 2008) have become increasingly popular for portable devices, due to high capacity and lifespan, relative safety, and tolerance for moderate discharge currents (up to ~2C) [2].

Consumer LIBs come pre-installed with special protection circuits as standard, which are designed to protect the cell from over-voltage, under-voltage, over-current, or thermal runaway conditions by isolating the cell. These devices dramatically improve the safety of Li-Ion cells by protecting the cells from misuse [1,3].

2.3 Modes of Failure and Fade

The SoH of LIBs does not remain constant over time and use, and instead suffer from capacity fade resulting from a combination of two major chemical processes within the cell.

The first ageing factor is the growth of Solid Electrolyte Film (SEF) upon the surface of the graphite anode. The SEF consists of a mix of Lithium Metal, Oxide and Carbonate, and grows thicker with time [8]. Not only does this process reduce the number of lithium charge carriers within the cell, but forms a barrier that resists the flow of the Li+ ions themselves and reduces the cell's ability to supply current [8]. This process occurs during discharge as Li+ ions move out of the graphite into the electrolyte and accelerates dramatically at low cell voltages (<2.5V) [2].

A similar film layer occurs at the cathode through a process known as Electrolyte Oxidation (EO) where, as the name implies, the electrolyte oxidizes, coating the cathode with a restrictive film that impedes ion flow [2]. EO is linked to operation of the cell at high voltages and temperatures, accelerating dramatically at cell voltages much above 4.1V [2]. In fact, research indicates that EO effects are generally the

dominant cause of capacity fade in consumer LIBs (due to lengthy times spent plugged in) [1].

It can be seen therefore that a stressful discharge (SEI) or spending a particularly long time at either a very high (EO) or very low voltage (SEI) are the primary accelerators of the ageing process. In light of this tradeoff, researchers believe a charge cut-off voltage of 3.92V (with 50% discharge depth) to be the sweet spot in terms of long life [2,3,8]. The result of which, however, is a maximum usable capacity on charge of only ~70% of the nominal capacity [2].

2.4 Modelling of Electrochemical Behaviour

The modelling of a battery's behaviour is an important area of research. Better mathematical models can help predict and simulate battery behaviour, by attempting to replicate the effects of the electrochemical processes within the cell. Randle's model, an adaption of which is shown in Figure 2, is commonly used for such analysis [2,9]. It consists of a DC voltage source, in series with parallel Resistive (R_P) and Capacitive (C_P) elements and an inline Resistance R_S. The inline Resistance R_S essentially represents the *fixed* resistance current flow within the cell (metal contacts, anode and cathode). The parallel elements (R_P and C_P) on the other hand change with both SoC and SoH, representing the effect of the electrolyte on Ion transfer. Essentially, R_P is the ease with which the electrolyte can transfer Ions between anode and cathode, while C_P represents the inertia of the cell that governs its reaction to changes in load current. It is these elements combined that result in the notable sudden drop in cell voltage upon loading (R_S and R_P) followed by the slow exponential curve (C_P) ending in a more linear drop as discharging continues. This is followed by a sharp bounce back upon going open-circuit followed by a slower recovery back to steady-state, as seen in Figure 13 in Section 4.3. This forms the basis for certain test modes, as discussed in Section 2.5.

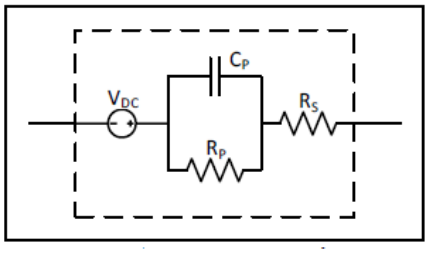

Fig.2: Randle's model of an electrochemical cell

2.5. Methods of Condition Estimation

This section explores several different and related methods of estimating the SoC and SoH of LIBs, each of which varies by complexity, speed and accuracy.

2.5.1 Static Measurements

Static measurements include *Open-Circuit Voltage* (OCV), *Cold Cranking Amps* (CCA), the slightly more relevant Maximum Instantaneous Power (MIP), and the derived Internal Resistance (IR). These tests share a similar level of complexity in that they can be run with simple equipment and require little analysis.

As a battery is discharged, its OCV will reduce slightly, and this can be used to give a rough estimate of the SoC [2]. A battery's ability to provide current also reduces as it is discharged and slightly with age [2]. CCA works by in effect shorting the battery terminals briefly through a shunt through which a value for maximum current can be established. This can then be used to indicate the SoC and SoH (assuming fully charged). MIP is similar but uses an electronic load to vary the resistance (to match the internal resistance) until the peak output power is reached. It should be noted that OCV, CCA, and MIP all require the cell to be unloaded and rested in order to get accurate results, plus CCA/MIP tests can be quite stressful upon the battery [7].

Finally, IR measures the DC Resistance of the cell (values R_P and R_S in Randle's Model covered in Section 2.4, which vary slightly with SoC and SoH) by measuring the current and voltage of a cell under load. Unlike the other measurements in this category this one can be monitored during operation using the load for the device.

The problem with using static measurements with LIBs is that, as previously mentioned, due to the challenge of a relatively flat discharge curve and near constant internal resistance, these methods (especially CCA/MIP/IR) prove unreliable and wildly inaccurate [2]. Research has shown that even in ideal circumstances the OCV method in LIBs has errors exceeding ±20% in SoC estimations [2].

2.5.2 Coulomb Counting

Coulomb Counting (or Current Integration) is perhaps the most common method of producing SoC and SoH estimations and is used by most common electronic devices [6]. The test is performed by applying a charge or discharge to the battery while monitoring the current across a shunt. By taking these measurements and simply integrating with respect to time (calculating the area under the curve) you can find the total charge transferred (Ah) in to and out of the cell. Hence calculating a cell's SoH, SoC and coulomb efficiency is a rudimentary problem of addition and subtraction. It follows that by also monitoring the cell voltage, you can easily find power flow with respect to time, integrating this to find the total energy transferred (Wh).

Coulomb Count is a relatively straightforward method to implement and requires relatively little analytical effort (cheap hardware-based integrator chips). The main factor affecting both complexity and accuracy of the measurement is naturally the frequency of monitoring. Low frequency measurements are easier to process but are more inaccurate due to integration errors and current fluctuation within the measurement period.

Systems built into devices (particularly those that are rarely subjected to a full discharge i.e. emergency lights), can also suffer from accumulative error [2]. This occurs as a result of the compounded errors from multiple partial cycles. To get the highest accuracy, the cell must be subjected to a full cycle

regularly providing an opportunity to reset the scale, and measure changes in the State of Health [10].

Laboratory-based Full Cycle Coulomb Counting (with measurement at a high frequency >10Hz) is naturally very accurate (±2% SoH/SoC), however researchers have found that in situ measurements can have error rates in excess of ±10% [6]. Temperature variations in typical use cases can also cause problems, reducing the current capability of the cells [1].
Researchers have had some success in Partial Cycle Coulomb Counting, where the cell is only discharged for a short period, and the curves extrapolated using mathematical models [11,12]. This has the benefit of significantly shorter test times, yet at the cost of a higher error rate than full cycle testing [11,12].

A number of mathematical methods have been used by researchers to increase the accuracy of both partial and full cycle measurements [11,13]. A notable example being Linear Quadratic Estimation (LQE, also known as Kalman Filtering), which uses mathematical models of batteries to better isolate and remove measurement error, to moderate effect [11,13].

2.5.3 Pulsed DC Load Analysis

Pulsed DC Load Analysis is essentially a more complex form measuring internal resistance of the cell by measuring the time taken for it to recover (reach steady-state) after a DC load has been removed. This essentially supplies a value to the influence of the Parallel Capacitive and Resistive elements in Randle's model covered in Section 2.4. As a cell loses charge, its inertia (ability to react to changes in current) increases, the same with SoH [2]. This is to say that the cell both fatigues faster and takes longer to recover from a stress.

The cell voltage and the time taken to get within a given range of the steady-state voltage is recorded after the load is removed. The resulting value can then be looked up on a chart formed from previous experimental data, and an estimate of the cell's SoC and SoH can be found.

Obviously, this form of test requires the battery to be taken out of service before it can be run. Additionally, studies have found large variations in recovery times across different cells (even from the same batch) due to natural variation in each cell's strength [2]. Cell-specific and model-specific lookup charts are generally required for SoC and SoH estimations, respectively, to obtain reliable results. In these cases, accuracies of up to ±15% SoC have been claimed [2].

2.5.4 Electrochemical Impedance Spectroscopy

Electrochemical Impedance Spectroscopy (EIS) is of particular interest to researchers [2,14]. It works by exciting cells with a low voltage, alternating current and measuring the complex impedance in the frequency domain (generally from 0.1-2000Hz). This permits the calculation of all elements within Randle's model. Researchers in this area have claimed extremely high accuracies of ±5% and ±10% for SoC and SoH estimations, respectively [2,14].

However, EIS testing is extremely difficult, measuring sub-milliohm level changes in complex impedance. This would require specialist equipment not readily accessible, namely an extremely low impedance, low frequency, a signal generator, a programmable electronic load, and a high precision oscilloscope so as to attain useful data with which to base the design of a more specialist test system.

3. METHOD AND MEASUREMENT

A design philosophy chosen at the beginning of the project was to create an accurate yet highly flexible test system that would automate the testing process in terms of control and measurement as much as possible. Automation would permit more extensive data to be collected with consecutive charge and discharge cycles, plus the flexibility to allow a wide range of speeds and forms of charge/discharge test to take place.

3.1 Test Hardware

The test system hardware consists of four major components: a computer, a microcontroller board, a USB data logger, and custom circuitry connecting to each test cell, an overview of which is shown in Figure 3. The computer controls the test cycle via a test program coded in MatLab©, reading in and storing precise voltage measurements via the USB data logger (National Instruments USB-6218 [15]) while outputting corrections via USB to the microcontroller (Microchip ATmega2560 based Arduino MEGA [16]). This interfaces with custom power and control circuitry to charge or discharge each cell (six in total) at the specified rate. Additionally, the microcontroller continuously monitors each cell for over-temperature condition, and cuts power to avert possible thermal runaway from a defective battery.

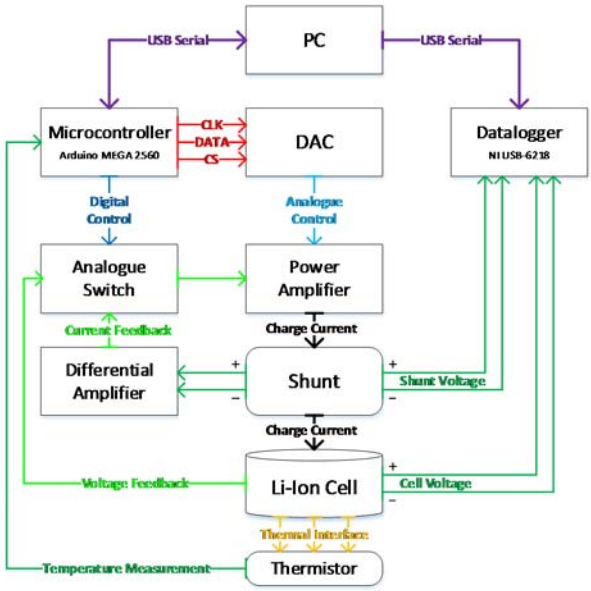

Fig.3: Block diagram of system hardware

3.1.1 Power

Power for the test system is provided from three sources:

1. The computer, which provides a *Single* Rail +5V supply via USB for the data logger, microcontroller, and custom circuitry.
2. A *Low* current (2A), *Dual* Rail ±12V bench source, providing an additional supply potential for Op-Amps within the custom circuitry.
3. A main *High* current (40A), *Single* Rail +5V bench source serves as a current source for charging cells.

Each cell is connected through a shunt resistor (0.05Ω, ±1%, 6W) for current measurement to a pair of matched MOSFETs, which form a high power "Push-Pull" amplifier.

The charge of each cell is controlled by operating the P-Channel MOSFET within its *Linear* region, controlling the resistance and thereby current, and dropping the voltage difference between the supply and cell in the process; in essence a *Linear Regulator*.

The discharge of each cell is controlled similarly by operating the N-Channel MOSFET within its *Linear* region, therefore resulting in a variable load, essentially forming a bespoke *Electronic Load* where the energy is dissipated by the MOSFET as heat.

A *Linear* approach for both charge and discharge was chosen because it produces naturally lower noise levels (compared with switch-mode designs), a high priority of laboratory based testing. Additionally, a *Linear* approach drastically reduced the circuit complexity required while meeting the high flexibility and control criteria required for laboratory based test system. It is expected that a switch-mode design, capable of recycling energy from cell discharge to offset supply requirements, could be implemented for mass operational testing. This option is at the cost of a more limited test regime as appropriate or more complex and costly design.

For safety and robust operation, all power components (especially MOSFETs) were chosen to handle the maximum design current of ±10A per cell while operating at well within tolerance.

3.1.2 Control

The test system is controlled though software on a computer, which determines the required current or voltage to be attained for each cell before sending this information to a microcontroller via a USB connection. The microcontroller then configures the custom control circuitry to set the charge/discharge rate, the circuit diagram for which can be seen in Figure 4.

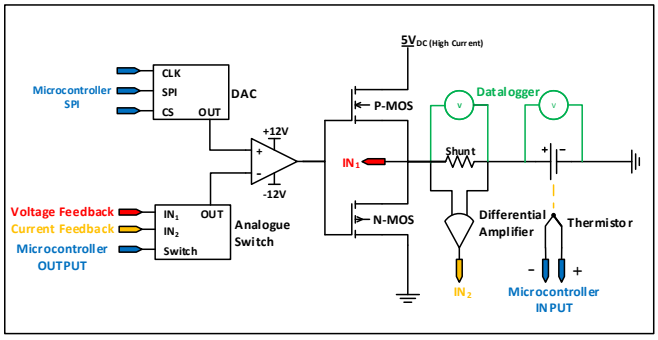

Fig.4: Circuit diagram of custom control circuit

At the heart of the Control system is a *Power Amplifier* (Op- Amp with a buffered output, forming a combination of linear regulator and electronic load). The system makes use of basic hardware feedback to maintain a desired charge/discharge rate (made suitable thanks to the comparatively slow response exhibited by LIBs). This feedback loop can be switched by a low impedance *Analogue Switch* between a voltage and current measurement. The current measurement is taken by way of a differential instrument amplifier and level shifter positioned across the shunt resistor. This permits either constant current or constant voltage operation, the control signal for which is provided by a DAC (12-bit, Analogue Reference: 4.4V, Accuracy: ±2LSB [16]) connected to the microcontroller.

3.1.3 Measurement

Experimental measurements of cell voltage and current are taken with the help of a high precision USB data logger (16x differential inputs, range: ±5V, full scale accuracy: ±1.41mV, sensitivity: ±47.2μV [15]), which feeds the measurements back to the software controller. This provides for much higher accuracy, precision and speed than would otherwise be attainable with the inbuilt microcontroller ADC [16]. This is important for computing accurate capacity estimations (as discussed in Section 3.2.2).

One of the 16 differential inputs is used to monitor the main power supply voltage to inform measures of internal power dissipation by the test circuit and prevent damage. A six cell test platform was chosen for implementation, with two differential inputs per cell. The first input measured the cell voltage and the second measured the voltage drop over the shunt resistor (converted into current by the software).

The data logger captures and returns reading from all inputs as a snapshot, and is capable of interfacing directly with MatLab© using the instrumentation tool (See Section 3.2.1). The data logger was recalibrated using a known voltage reference source before use and an Ohmic standard was used to accurately measure the actual value of each shunt resistor to a finer tolerance (within ±0.1%).

The ADC functionality of the microcontroller is made use of, however, as a safety system to measure the temperature of each cell and MOSFETs (within a few degrees Celsius) using thermistors. When a high thermal condition is detected (indicating a defective cell or component failure) the microcontroller will automatically cut current to avert thermal runaway or other damage. This replicates the protection circuits built into LIBs and permits the *safe testing* of LIBs without their safety circuits (which otherwise might introduce transient loads and impedances that affect the validity of the electrochemical mode, see Section 2.4).

3.2 Test Software

The test software has been designed using MatLab©. This simplified coding and data processing by enabling results to be both collected and processed within a single environment.

The MatLab© instrumentation toolbox also makes interfacing with external devices a simple process. Though MatLab© is a popular software in research settings, it also supports exporting as an executable file for systems without a MatLab© license. The software is separated into two parts to streamline execution and to simplify use. Together, they form a simple, unified test control mechanism that can be built upon and adapted for future deployments or implementations.

3.2.1 Control and Measurement

The Test Controller manages the testing of cells, determines the charge/discharge current, and records the experimental data for later processing. The basic flow and sub-functions are shown in Figure 5. After initial setup, the Test Controller loop begins to run. At the beginning of each loop, the software reads in a snapshot of measurements from the data logger, before analyzing each cell in turn and calling the appropriate Test Controller sub-routine (see Section 3.3) dependent on the mode of test selected (if any).

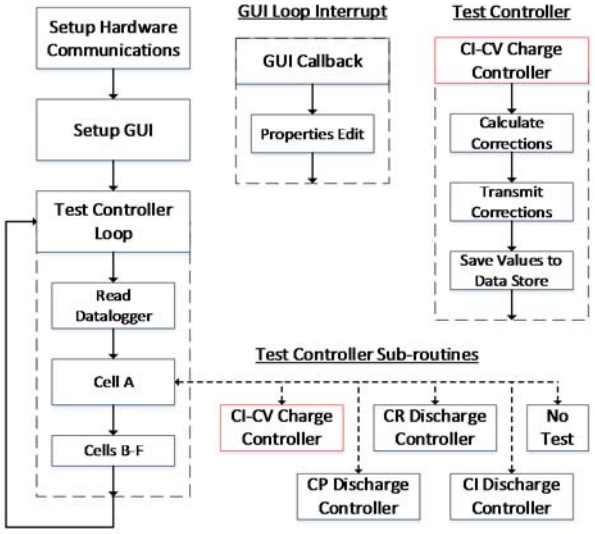

Fig.5: Block diagram of system control software operation

More streamlined control of the test system was achieved by means of a Graphical User Interface (GUI) as shown in Figure 6.

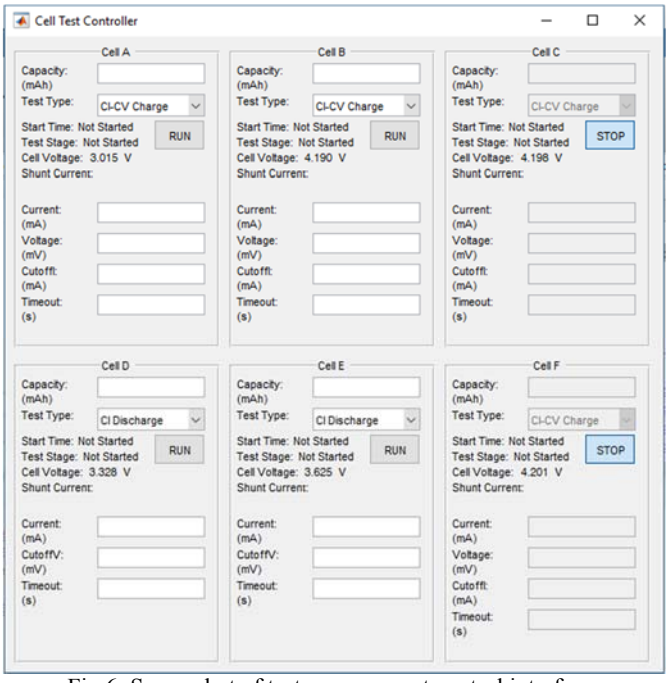

Fig.6: Screenshot of test management control interface

This allowed for a more straightforward setup and configuration of test cycles while reducing accidental setup errors and providing basic status information during the test cycle. Clicking run on the GUI triggers a callback that automatically transfers the test properties ready for enactment during the next Test Controller loop execution.

3.2.2 Processing and Analysis

In order to ensure fast execution of the Test Controller part of the software system, unnecessary computations are kept to a minimum, for example, unit conversions i.e. shunt voltage measurements to current. The Data Processing tool fulfills this further processing requirement and contains sub-routines for additional processing, for example, data smoothing and capacity/SoH/SoC measurement (using integration over the charge/discharge curve). The processing routines make use of many of the built-in MatLab© functions to efficiently process and display data with minimum user effort. To simplify the process again when processing multiple varied datasets, a GUI was designed to merge the different data processing sub-routines within a single interface, shown in Figure 7.

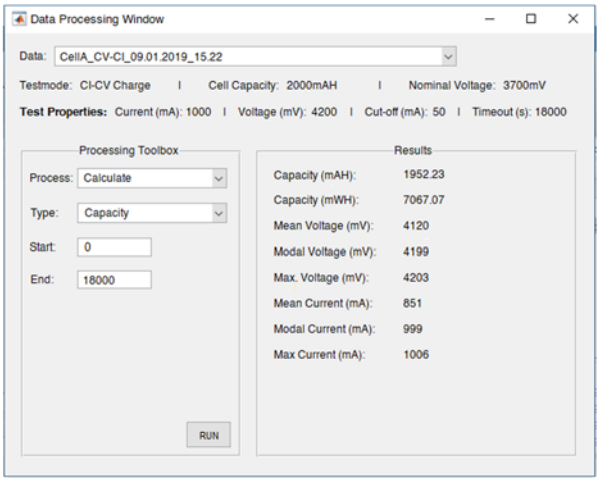

Fig.7: Screenshot of data processing interface

3.3 Modes of Test

Various test modes have been programmed to enable analysis of LIBs, the most significant of which are outlined here.

3.3.1 Charge: Constant Current – Constant Voltage

Although the test system is capable of other charging approaches, LIBs are normally charged in a 2-stage process known as Constant Current – Constant Voltage (CI-CV) charge, of which a diagram is shown in Figure 8. It is therefore logical to use this charge process in experimentation.

At a low SoC, the LIB will readily accept current, and a set *Constant Current* (CI, ideally <1C) is therefore applied to the cell, which gradually raises (after an initial jump) the cell voltage in near linear fashion until the supply reaches a set *Charge Cut-off Voltage* (CCV, normally set at 4.2V as discussed in Section 2.3). At this point, the supply switches to *Constant Voltage* (CV) mode for a period known as *Saturation Charge*. During saturation, the current into the cell slowly drops as the internal potential slowly rises towards the supply. When the current drops below a set point (generally around 0.03C), the supply is switched off, as allowing a LIB to *float* is extremely damaging to Li-Ion cells (a result shown in Section 4.2.1).

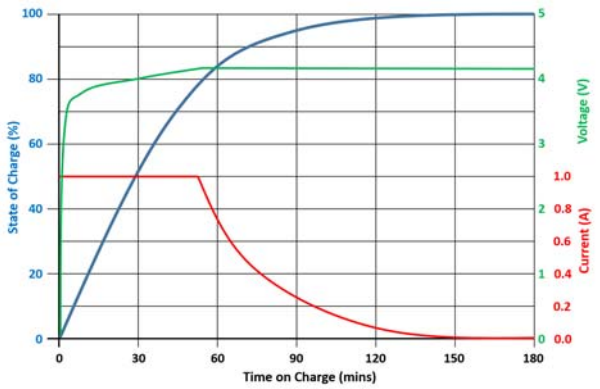

Fig.8: Standard CI-CV Li-Ion charge cycle [2]

The SoC gained and length of each stage depends on the charge current. The higher the current the faster the cell will reach cut-off, but the lower the maximum SoC attainable. This is the reason an electric vehicle can charge to 70% SoC in 30mins, but takes much longer to reach 100%.

3.3.2 Discharge: Constant Current/Load/Power

The specific format a discharge cycle takes varies wildly between applications and is rarely constant in nature. A cell phone, for example, typically draws current for short intervals when in use, and when communicating with its network. However, constant discharge measurements are simpler and more definable in terms of analysis. These discharge modes take three natural forms: *Constant Current* (CI), *Constant Power* (CP), and *Constant Load*/Resistance (CR).

CI discharge is the simplest experimentally and replicates the demands of a linear regulator driving a constant load, where the drawn current will remain constant irrespective of voltage. CP discharge replicates the demands of a switch-mode regulator driving a constant load, where the current drawn will increase as the cell voltage drops in order to maintain a power to the load. Finally, CR discharge replicates the response of a resistive component attached directly to a cell, where the current draw will decrease in line with Ohm's Law as the cell voltage drops.

These tests provide an ideal basis for Coulomb Counting SoH and SoC estimation as the changes in cell voltage remain relatively steady with time, reducing the errors in the numerical integration.

3.3.3 Pulsed DC load and Recovery

As outlined in Section 2.5.3, a Pulse DC Load Test applies a *stress* (set CI/CP/CR discharge) to a cell for a set *duration* (normally a few seconds) until the rate of change in cell voltage becomes approximately linear. The stress load is then removed and the recovery of the battery measured until the cell returns to steady-state. Properties of interest are the *recovery voltage* (difference between loaded and open-circuit voltage at steady-state) and *recovery time* (time taken to reach steady-state), which are automatically extracted from the datasets by the Data Processing tool. A strong battery in terms of SoC and SoH should cope better with a given stress than a weaker battery. By analysis of this data across multiple cells, estimations of SoC and SoH can be derived with a much shorter test than is possible with Coulomb Counting, at the cost of accuracy.

4. VERIFICATION AND ANALYSIS

In this section, details of the result of experiments into SoH and SoC estimations are used to verify the operation and functionality of the test system.

4.1. Control of Test Conditions

An important consideration in the design of the test system was in minimizing the noise levels that could otherwise affect

the quality of the test data. It can be seen from Figure 9 that the noise of the test system in operation is relatively low, with over 99% of readings within ±1mV of the mean. Smoothing by moving average is effective at reducing this noise level significantly with a 10 and 100 point (~1s and ~10s) reducing signal jitter to within 0.4mV and 0.1mV, respectively.

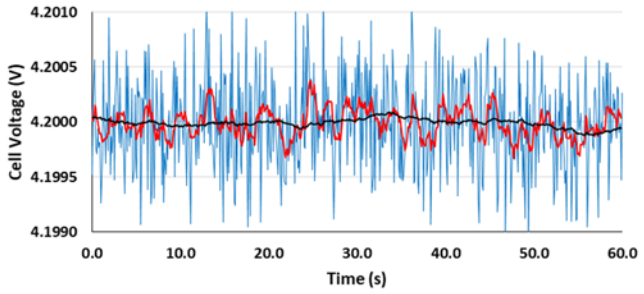

Fig.9: Measurement noise in test system

4.2 State of Health Estimation

In order to demonstrate the effect of the rate of discharge on useful capacity, a 2Ah nominal capacity, 18650 NMC LIB was discharged at various C-Rates (CI) down to a low cut-off of 2.5V. The cell was charged using the CI-CV method at 0.5C to 4.2V and rested before each discharge, while Coulomb Counting was used to monitor the energy extracted. The result of which can be seen in Figure 10.

It can be seen that with gentler discharges (<0.5C) the cell voltage remains relatively constant at around the nominal voltage (3.7V) across the main body of the discharge, dropping sharply at the very end. It can be noted therefore that at gentle discharge the selection of a higher cut-off voltage does not have a great effect on the useful charge extracted. However, as the rate increases the cell begins to struggle and the cell voltage drop occurs earlier in the discharge, eventually approaching linear as the cell can no longer keep up. At high discharge rates we can note that higher cut-off voltages will significantly reduce the extractable capacity (1Ah at 3V vs 1.7Ah at 2.5V).

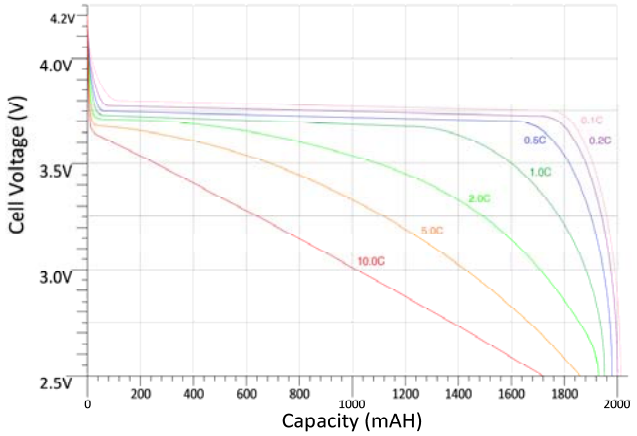

Fig.10: Cell voltage given measured capacity at various rates of discharge

4.2.1 Charge: Constant Current- Constant Voltage

In order to identify the effect of discharge rate of SoH, three new 2Ah nominal capacity, 18650 NMC LIBs were subjected to repeated cycling at different discharge rates (CI to 3V) with the measured SoH calculated by Coulomb Counting on each discharge. The results are shown in Figure 11. Again, each cell was charged using the CI-CV method at 0.5C to 4.2V and rested before each discharge.

It can be seen that even over a modest number of cycles there is a distinct drop in capacity. The effect of higher discharge rates can also be seen, with the cell discharged at 1C, losing a total capacity of 3.7% vs 1.5% when discharged at 0.2C (though the small sample size should be kept in mind).

Another notable feature is the variance in the measured capacity between successive tests. This is to be expected due to the imperfect nature of the battery and the effect of environmental factors, as well as a small compounded effect of errors from numerical integration.

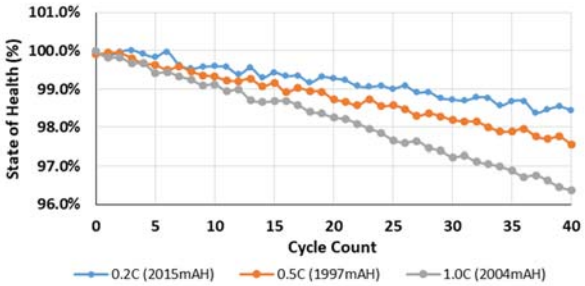

Fig.11: Change in SOH per cycle, at different discharge rates

4.2.2 Charge Voltage

As discussed in Section 2.3, a major accelerator of capacity fade is charge voltage. In order to study the effects of charge voltage on capacity fade, four 2Ah nominal capacity, 18650 NMC LIBs were subjected to 30 charge/discharge cycles. Cells were charged using the CI-CV method (at 0.5C) to set cut-off voltages, before discharging (at 0.5C) to 3.0V. Cells were rested for a similar period in between charge and discharge, and the capacity was measured using Coulomb Counting during each discharge. The results are displayed in Figure 12. Note that to better illustrate the change in State of Health, capacities are relative to the initial measured capacity at the given charge voltage, as charge voltage affects the usable capacity of the cell.

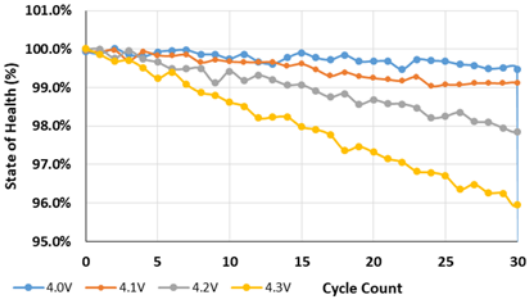

Fig.12: Effect of charge voltage on state of health

Looking at the graph, there is a clear negative correlation between charge voltage and its effect on State of Health, as expected. Particularly evident is the dramatic increase in capacity fade at a charge voltage of 4.3V when (as discussed in Section 2.3) the process of Electrolyte Oxidation starts to accelerate. Extrapolating the rate of capacity fade when charging to 4.3V predicts "end-of-life" (80% SoH) at only ~150 cycles. Likewise dropping from the "standard" charge voltage of 4.2V to 4.1V more than doubles the cycle count at the cost of just over 10% usable capacity. This data therefore supports the option implemented in some devices, e.g. electric cars, to reduce charge voltage unless maximum capacity is specifically required, a system that has the potential as shown to dramatically increase battery longevity [2,5].

4.2.3 Cycle Efficiency

To examine the effect of charge and discharge rate on cycle efficiency, five 2Ah nominal capacity, 18650 NMC LIBs were charged (to 4.2V) and discharged (to 3.0V) at a selection of rates, resting cells between each discharge. The energy transferred is then computed using Coulomb Counting, and the cycle efficiency calculated. The tabulated results are shown in Table 2.

Table 2: Tabulated results of LIB cycle efficiency

Charge / Discharge	0.2C	0.5C	1.0C
0.2C	98.11 (σ=11)	97.69 (σ=17)	97.02 (σ=18)
0.5C	97.22 (σ=15)	96.75 (σ=19)	95.87 (σ=21)
1.0C	96.24 (σ=19)	95.59 (σ=22)	94.71 (σ=31)

It can be seen from the table that the more stress the battery receives in terms of either charge or discharge current, the less efficient the battery becomes. Generally, the efficiency of the cell is not as high as might be expected, however this may be down to the age of these particular cells, and performance is still significantly greater than other chemistries. It should be noted that the efficiencies are specifically for the cell, and exclude circuit losses.

4.3 State of Charge Estimation

For the purpose of State of Charge estimation, experiments to ascertain the potential of DC Pulse Load Analysis were conducted. A 2Ah nominal capacity, 18650 NMC LIB was subjected to multiple constant current (1C) discharges of 5% of the measured capacity (cut-off 3V, approximately 150s duration with 19 in total). The discharge was stopped and the cell rested while the rate of recovery was measured. Discharge was resumed when the cell's OCV reached a steady-state. After the final discharge period, the cell was charged using the CI-CV method at 0.5C to 4.2V and rested before repeating. The condensed result of one discharge cycle is shown in Figure 13 below, where the increasing recovery period can be clearly seen.

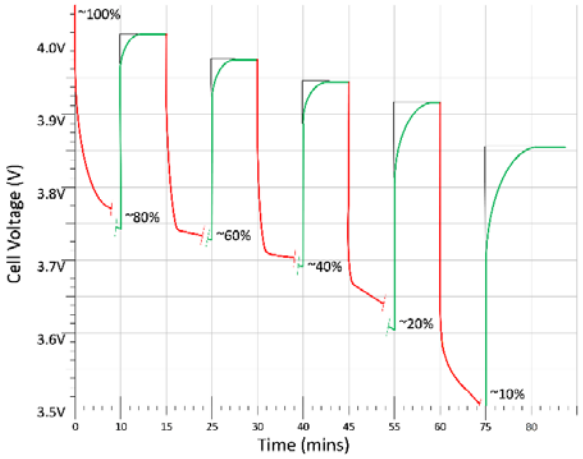

Fig.13: Recovery period of LIB post loading across various SoC

The tabulated results showing the measurements of the recovery period for 20 cycles (of 19x Pulsed Discharges and Recovery Periods) is shown in Table 3.

It can be seen from the changes in mean values that the recovery time increases as the cell is discharged, conversely the steady-state voltage decreases. The recovered and lost voltages actually start by decreasing slightly before staying steady, then increase sharply toward full discharge. It can be noted by examining the change in mean and standard deviation of the steady-state voltage and recovery time, that recovery time (as expected) has the biggest ratio of mean changes to data variance. That is the most significant change compared to the overall variance in the dataset, and therefore a good candidate for trend setting.

Table 3: Tabulated results of pulsed discharge analysis of LIB

Discharge Depth (%)	Steady-State Voltage (mV)	Average Recovery Time (s)	Average Recovered Voltage (mV)	Average Lost Voltage (mV)
5%	4187 (σ=7)	89 (σ=9)	414 (σ=29)	422 (σ=27)
20%	4009 (σ=11)	126 (σ=11)	272 (σ=24)	273 (σ=21)
40%	3974 (σ=13)	154 (σ=15)	249 (σ=18)	271 (σ=21)
60%	3948 (σ=17)	192 (σ=18)	260 (σ=20)	269 (σ=25)
80%	3923 (σ=19)	239 (σ=21)	318 (σ=32)	380 (σ=28)
90%	3856 (σ=24)	314 (σ=26)	550 (σ=64)	609 (σ=47)
95%	3761 (σ=41)	426 (σ=33)	891 (σ=89)	928 (σ=76)

Using these results, it therefore possible to reverse the data and predict SoC based on recovery time, setting a 95% confident interval (two standard deviations). This forms the lookup chart shown in Figure 14. It can therefore be seen that for this cell there is an expected accuracy for SoC estimations

of between ±4% and ±18%, depending on the SoC itself. In a similar fashion to recovery time, the use of steady-state voltage can produce an expected accuracy for SoC estimations of between ±3% and ±28%.

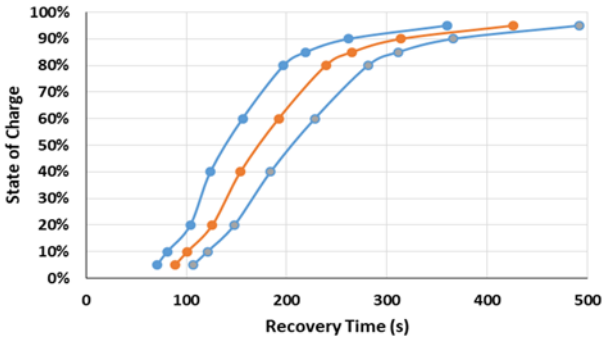

Fig.14: Expected state of charge for a given recovery time

In order to improve accuracy and make use of the different measurements that are collected as part of the same test. Pearson's Product-Moment can be used to establish the degree of correlation between the two measurements. Analysis indicates a correlation coefficient of -0.42 between steady-state voltage and recovery time. Using this fact, it is therefore possible to increase the accuracy of predictions slightly to between ±2% and ±16% at 95% confidence, given the experimental data.

5. CONCLUSIONS

The testing has been undertaken on a single product line of LIB, and therefore the accuracy of prediction results cannot be expected to hold for other LIBs. However, this test system can be used to create a suitable comparison set for other batteries. Attempts at facilitating EIS of LIBs were made, however further work is needed to permit the measurement sensitivity and control precision required for the effective EIS of LIBs. The changes in impedance are in the range of 10's of milliohm, and therefore very difficult to detect while keeping excitation currents low. This would likely require the use of additional cost prohibitive laboratory equipment, including high precision electronic loads and high current, low frequency signal generators to facilitate initial analysis.

For this project a flexible and accurate test system has been designed and built, and the operation verified and results analyzed. The effect of different usage patterns on SoH has been shown and Pulse DC Analysis has been used to estimate SoC.

It is hoped that the research outlined in this paper will help in the development of more comprehensive experimental datasets and accompanying understanding of LIBs, in that the test system design proposed might be built upon and improved, perhaps with additional testing routes or capability to conduct EIS measurements.

REFERENCES

[1] Butterworth-Heinemann, Rechargeable battery applications handbook. Gates Energy Products, 1992.

[2] I. Buchmann. Batteries in the Portable World, 4th Ed. Cadex Electronics, 2016. ISBN: 978-0968211847, p151-200, 320-340.

[3] D. Linden. Handbook of batteries, 2d Ed. McGraw-Hill, 1995.

[4] B. Scrosati, et el. Lithium batteries: status, prospects and future. Journal of Power Sources, v195, p2419-2430, 2010.

[5] Lithium-Ion Batteries: Fundamentals and Applications. IEEE Industrial Electronics Magazine, v10, p58-59, 2016.

[6] M. Berecibar, et el. Critical review of state of health estimation methods of LIBs for real applications. Renewable and Sustainable Energy Reviews, v56, p572-587, 2016.

[7] M. Fleischhammer, et el. Interaction of cyclic aging at high-rate and low temperatures and safety in lithium-ion batteries. Journal of Power Sources v274, p432-439, 2015.

[8] S. Choi, et el. Factors that affect cycle life and possible degradation mechanisms of lithium ion batteries based LiCoO2. Journal of Power Sources, v111, 2002

[9] S. Rael, et el. Using electrical analogy to describe mass and charge transport in lithium-ion batteries. Journal of Power Sources, v222, p112-122, 2013.

[10] Z. Guo, et el. State of health estimation for lithium ion batteries based on charging curves. Journal of Power Sources, v249, p457-462, 2014.

[11] S. Sepasi. Inline state of health estimation of lithium-ion batteries using state of charge calculation. Journal of Power Sources, v299, p246-254, 2015.

[12] A. Eddahech, et el. Determination of Lithium-ion battery state-of-health based on constant-voltage charge phase. Journal of Power Sources, v258, p218-227, 2014.

[13] S. Sepasi. Improved extended Kalman filter for state of charge estimation of a battery pack. Journal of Power Sources, v255, p368-376, 2014.

[14] L. Ran, et al. Prediction of state of charge of lithium-ion rechargeable battery with electrochemical impedance spectroscopy theory. Industrial Electronics and Applications, 5th IEEE Conference, 2010.

[15] National Instrument. USB-6218 Specification. www.ni.com/pdf/manuals/375199d.pdf. Accessed: 29/04/2019.

[16] Microchip ATmega2560 Datasheet. www.microchip.com/downloads/en/DeviceDoc /ATmega640-1280-1281-2560-2561-Datasheet-DS40002211A.pdf. Accessed: 29/04/2019.

[17] Tesla Model S Manual. www.tesla.com/sites/default/files/model_s _owners_manual_north_america_en_us.pdf. Accessed: 29/04/2019.